Hindawi
International Journal of Aerospace Engineering
Volume 2021, Article ID 6657281, 19 pages
https://doi.org/10.1155/2021/6657281

Research Article

Sliding Mode Control Based on High-Order Linear Extended State Observer for Near Space Vehicle

Ouxun Li,[1,2] **Ju Jiang**,[1] **Li Deng**,[2,3] **and Shutong Huang**[1,2]

[1]*Nanjing University of Aeronautics and Astronautics, Nanjing 211106, China*
[2]*Guilin University of Aerospace Technology, Guilin 541004, China*
[3]*University of Electronic Science and Technology of China, Chengdu 611731, China*

Correspondence should be addressed to Ouxun Li; liouxun@guat.edu.cn

Received 6 October 2020; Revised 1 January 2021; Accepted 9 January 2021; Published 10 February 2021

Academic Editor: James D. Biggs

Aiming at the uncertainty and external disturbance sensitivity of the near space vehicles (NSV), a novel sliding mode controller based on the high-order linear extended state observer (LESO) is designed in this paper. In the proposed sliding mode controller, the double power reaching law is adopted to enhance the state convergence rate, and the high-order LESO is designed to improve the antidisturbance ability. Moreover, the appropriate observer bandwidth and extended order are selected to further reduce or even eliminate the disturbance by analyzing their influences on the observer performance. Finally, the simulation demonstrations are given for the NSV control system with uncertain parameters and external disturbances. The theoretical analyses and simulation results consistently indicate that the proposed high-order LESO with carefully selected extended order and observer bandwidth has better performance than the traditional ones for the nonlinear NSV system with parametric uncertainty and external disturbance.

1. Introduction

Near space vehicle (NSV) has many excellent characteristics, such as fast speed, strong survival and penetration ability, high flight altitude, wide application range, and strong precision strike ability. Despite the great challenges of NSV control considering the nonlinearity, strong coupling and uncertainty of NSV, in addition with their susceptibility to external disturbances [1], the control technology based on modern control theory has been widely studied. Morden control methods such as the robust control, predictive control, sliding mode control, and intelligent control have been applied to hypersonic vehicle control and achieved certain results. On the other hand, the single control method has its own advantages and disadvantages in the NSV control application, which might not meet the multiple requirements of flight control. Therefore, the combination of different control methods to give full play to their respective advantages has become one of the research focus.

In practical applications, uncertainties such as modeling errors and external disturbances are always existent, which make the system output unstable or asymptotically track the desired target. Therefore, different robust control strategies have been proposed. Thereinto, the sliding mode control has been widely used in the flight control system due to its simple structure, fast response, and its insensitivity to external disturbances [2, 3]. In [4], a finite-time attitude control is developed to ensure that the required thrust vector is met exactly at the prescribed time. In [5], a novel recursive singularity free fast terminal sliding mode strategy for finite-time tracking control of nonholonomic systems is proposed. Specially, the sliding mode control with disturbance observation compensation is quite suitable for uncertain nonlinear systems with external disturbances and parameter perturbations [6, 7]. In [8], a novel nonsingular fast terminal sliding mode control method based on disturbance observer is proposed for the stabilization of the uncertain time-varying and nonlinear third-order systems. In [9], the uncertainties are effectively solved by the combination of the sliding mode control and the interval type-2 Takagi-Sugeno-Kang (TSK) fuzzy control. The double power reaching law sliding mode control is adopted in [10] to track the large range command of the

climbing stage of the NSV for better performance. In the aspect of anti-interference, the extended state observer can estimate the total disturbance in real time according to the input and output system information and can be eliminated in the feedback control, so that the closed-loop dynamic system has better control performance. Moreover, there is a set of mature empirical formula for the parameter tuning of the observer, which is more convenient for engineering application. In [11], a robust adaptive finite-time fast terminal sliding mode controller is proposed to achieve the desired formation in the presence of model uncertainties and external disturbances. In [12], a novel sliding mode control approach is proposed for the control of a class of underactuated systems which are featured as in cascaded form with external disturbances. Authors in [13] proposed a combination of finite-time robust-tracking theory and composite nonlinear feedback approach for the finite-time and high-performance synchronization of the chaotic systems in the presence of the external disturbances, parametric uncertainties, Lipschitz nonlinearities, and time delays. In [14], an adaptive controller is proposed by employing an event-triggered control and an extended-state-observer, where a simple strategy to tune the observer parameters is provided. Authors in [15] compensate the disturbance by combining the sliding mode control with the autodisturbance rejection control. A novel antisaturation controller is designed in [16] for the air breathing hypersonic vehicle, using the observer to compensate the mismatched disturbance. A state observer with adaptive extension and a continuous sliding mode controller with disturbance observer are proposed and applied to the hypersonic vehicle system in [17, 18], respectively. The nonlinear disturbance observer is applied to the robust flight control of the air breathing hypersonic vehicle in [19], which can significantly improve the robustness and antidisturbance ability of the system. Authors in [20, 21] have pointed out that the high-gain error feedback can guarantee the fast convergence of the observation error and the sufficient estimation accuracy. The performance analyses of the LESO and its higher order form for the second-order system in [22] indicate that the high-order form has faster response speed and better low-frequency characteristics.

From the above recent works, it can be seen that the sliding mode control has good robustness in the NSV control system. The disturbance observation compensation can reduce or even eliminate the disturbance and improve the antidisturbance ability. However, considering the high-order, uncertainty, strong coupling of the NSV control system and other factors in the practical application, the traditional LESO could not meet the performance requirements of NSV control system. Given that, a novel sliding mode controller based on the high-order LESO is proposed in this paper. Based on the traditional LESO method, the high-order LESO is used to estimate and compensate the external disturbance. The sliding mode control method with disturbance compensation is used to improve the stability and anti-interference ability of the system. In this paper, we have proven that compared with the traditional LESO, the high-order LESO has better low-frequency characteristics and anti-disturbance ability for the NSV control system. The main contributions of our work can be concluded as follows.

(1) The feedback linearization equivalent model of NSV is established. According to the equivalent model, a sliding mode controller with high-order disturbance compensator is designed to improve the system stability and anti-interference ability. The convergence region of high-order disturbance observer under the condition of lumped disturbance is analyzed, and the system stability is also proved by Lyapunov method

(2) The sliding mode controller with high-order LESO compensation is proposed, and the design method of the high-order LESO is also provided

(3) The transfer functions from the lumped disturbance to the disturbance estimate and the disturbance estimate error in high-order form are deduced, respectively. Moreover, the influence of the observer bandwidth and the extended order on the observer performance are analyzed specifically in the time domain and frequency domain, respectively

(4) The nonlinear NSV model with uncertain parameters and external disturbance has been proven, and the simulation results also show that the high-order LESO has better robustness and antidisturbance ability by selecting appropriate order and observation bandwidth

The remainder of this paper is organized as follows. The theoretical bases are presented in Section 2, including the NSV modeling, the sliding mode controller, and the traditional observer design method. The proposed high-order LESO is detailed in Section 3. The aircraft case simulations and discussions are provided in Section 4, followed by the conclusion in Section 5.

2. Preliminaries

2.1. NSV Model. According to [9] and [23–26], the motion model of NSV longitudinal channel is defined as follows:

$$\begin{cases} \dot{v} = \dfrac{T\cos\alpha - D}{m} - \dfrac{\mu\sin\gamma}{r^2}, \\ \dot{\gamma} = \dfrac{L + T\sin\alpha}{mv} - \dfrac{\left(\mu - v^2 \mathrm{r}\right)\cos\gamma}{vr^2}, \\ \dot{q} = \dfrac{M_y}{I_y}, \\ \dot{\alpha} = q - \dot{\gamma}, \\ \dot{h} = v\sin\gamma, \\ \ddot{\beta} = -2\xi\omega\dot{\beta} - \omega^2\beta + \omega^2\beta_c, \end{cases} \tag{1}$$

where v, γ, q, α, and h indicate the velocity, track angle, pitch rate, angle of attack, and altitude, respectively; β, ω, and ξ are

severally the throttle setting, engine natural frequency, and damping coefficient, followed by L, D, T, m, μ, r, M_y, and I_y as the lift, drag, thrust, mass, gravitational constant, distance from the center of mass to the center of gravity, pitching moment, and the moment of inertia, respectively. Thereinto, the lift, drag, and thrust can be expressed as [9]

$$\begin{cases} L = \dfrac{1}{2}\rho v^2 \mathrm{s} C_L, \\ D = \dfrac{1}{2}\rho v^2 \mathrm{s} C_D, \\ T = \dfrac{1}{2}\rho v^2 \mathrm{s} C_T, \\ C_m(\delta_e) = 0.0292(\delta_e - \alpha), \\ M_y = \dfrac{1}{2}\rho v^2 \mathrm{s}\bar{\mathrm{c}}(C_m + C_m(\delta_e)), \\ C_T = \begin{cases} 0.02576\beta, & \beta < 1, \\ 0.0224 + 0.00336\beta, & \beta \geq 1, \end{cases} \end{cases} \tag{2}$$

where C_L, C_D, C_T, and C_m are coefficients for the lift, drag, thrust, and pitch moment, respectively; the control input signals include the throttle setting β_c and elevator deflection angle δ_e.

Note that the NSV model in Equation (1) is nonlinear. However, according to the nonlinear theory, the input-output linearization can be adopted first; then, v and h are derived three times and four times, respectively. Thus, the linearized model can be obtained as follows [9]:

$$\begin{cases} \dot{v} = \dfrac{T\cos\alpha - D}{\mathrm{m}} - \dfrac{\mu \sin\gamma}{\mathrm{r}^2} = f_1(x), \\ \ddot{v} = \dfrac{\partial f_1(x)}{\partial \mathrm{x}}\dot{x} = \omega_1 \dot{x}, \\ \dddot{v} = \dot{x}^T \dfrac{\partial \omega_1}{\partial x}\dot{x} + \omega_1 \ddot{x} = \omega_1 \ddot{x} + \dot{\mathrm{x}}^{\mathrm{T}} \omega_2 \dot{x}. \end{cases} \tag{3}$$

$$\begin{cases} \dot{h} = v \sin\gamma, \\ \ddot{\mathrm{h}} = \dot{\mathrm{v}} \sin\gamma + v\dot{\gamma}\cos\gamma, \\ \dddot{\mathrm{h}} = \ddot{\mathrm{v}} \sin\gamma + 2\dot{\mathrm{v}}\dot{\gamma}\cos\gamma - \mathrm{v}\dot{\gamma}^2 \sin\gamma + \mathrm{v}\ddot{\gamma}\cos\gamma, \\ h^{(4)} = \ddot{\mathrm{v}} \sin\gamma + 3\ddot{\mathrm{v}}\dot{\gamma}\cos\gamma - 3\dot{\mathrm{v}}\gamma^2 \sin\gamma + 3\dot{\mathrm{v}}\ddot{\gamma}\cos\gamma - \mathrm{v}\dot{\gamma}^3 \cos\gamma - 3\mathrm{v}\dot{\gamma}\ddot{\gamma}\sin\gamma + \mathrm{vcos}\gamma\dddot{\gamma}, \end{cases} \tag{4}$$

where the first, second, and third derivatives of γ are obtained according to Equation (1) as

$$\begin{cases} \dot{\gamma} = \dfrac{L + T\sin\alpha}{mv} - \dfrac{\left(\mu - v^2 r\right)\cos\gamma}{vr^2} = f_2(x), \\ \ddot{\gamma} = \dfrac{\partial f_2(x)}{\partial \mathrm{x}}\dot{x} = \pi_1 \dot{x}, \\ \dddot{\gamma} = \dot{\mathrm{x}}^T \dfrac{\partial \pi_1}{\partial x}\dot{x} + \pi_1 \ddot{x} = \pi_1 \ddot{x} + \dot{\mathrm{x}}^T \pi_2 \dot{x}, \end{cases} \tag{5}$$

where $\omega_1 = \partial f_1(x)/\partial x$, $\omega_2 = \partial \omega_1/\partial x$, $\pi_1 = \partial f_2(x)/\partial x$, and $\pi_2 = \partial \pi_1/\partial x$.

Note that in Equation (3) and Equation (5), the flight state vector $\mathbf{x} = [v\ \gamma\ \mathrm{q}\quad \alpha\quad h]^T$ is available for measurement. Accordingly, the linearized model can be described as follows:

$$\begin{cases} \ddot{\mathrm{v}} = F_V + b_{11}\beta_c + b_{12}\delta_e, \\ h^{(4)} = F_h + b_{21}\beta_c + b_{22}\delta_e. \end{cases} \tag{6}$$

$$\begin{cases} F_v = \dfrac{\omega_1 \ddot{x}_0 + \dot{x}^T \omega_2 \dot{x}}{\mathrm{m}}, \\ F_h = 3\dot{v}\dot{\gamma}\cos\gamma - 3\dot{v}\gamma^2 \sin\gamma + 3v\dot{\gamma}\dot{\gamma}\cos\gamma - v\dot{\gamma}^3\cos\gamma - 3v\dot{\gamma}\dot{\gamma}\sin\gamma \\ + \dfrac{\omega_1 \ddot{x}_0 + \dot{x}^T \omega_2 \dot{x}}{m} \sin\gamma + v\cos\gamma\left(\pi_1 \ddot{x} + \dot{x}^T \pi_0 \dot{x}\right), \\ b_{11} = \dfrac{\rho v^2 s C_\beta \omega^2}{2m} \cos\alpha \\ b_{12} = -\dfrac{\rho v^2 s\bar{c} \bullet c_e}{2mI_y}(T\sin\alpha + D_\alpha), \\ b_{21} = \dfrac{\rho v^2 s C_\beta \omega^2}{2\mathrm{m}} \sin(\alpha+\gamma) \\ b_{22} = \dfrac{\rho v^2 s\bar{c} \bullet c_e}{2mI_y}(T\cos(\alpha+\gamma) + L_\alpha \cos\gamma - D_\alpha \sin\gamma) \end{cases} . \tag{7}$$

When the external disturbances are considered, the linearized model can be uniformly described as [27, 28].

$$\begin{bmatrix} \ddot{v} \\ h^{(4)} \end{bmatrix} = \begin{bmatrix} F_v \\ F_h \end{bmatrix} + \mathbf{B}\,\mathbf{U} + \begin{bmatrix} d_1(t) \\ d_2(t) \end{bmatrix}, \tag{8}$$

where $\mathbf{U} = [\,U_1 \quad U_2\,]$, and β_c and δ_e in Equation (6) are substituted by U_1 and U_2 as the control inputs. This linearized model considering external disturbances of Equation (8) is defined under the hypotheses as follows [28]:

Assumption 1. The external disturbance $d_i(t)$ and its first-order differential are bounded as $|d_i(t)| \le \delta$, $|\dot{d}_i(t)| \le \bar{\delta}$, where δ and $\bar{\delta}$ are known normal numbers.

Assumption 2. The matrix B is nonsingular. In the whole branch envelope, it is reasonable to assume that the matrix B is nonsingular because the flight path angle of the aircraft satisfies $\gamma \ne \pm\pi/2$.

Note that Assumption 1 is only suitable for the traditional state expansion observer. The high-order form of observer will be discussed in the following sections.

2.2. Design of the Sliding Mode Controller. The design process of the sliding mode controller can be described as the following two steps.

(1) Select the integral sliding surface $\mathbf{S} = [\,S_v \quad S_h\,]$ as

$$\mathbf{S} = \begin{cases} S_v = \left(\dfrac{d}{dt} + \lambda_v\right)^3 \displaystyle\int_0^t e_v(\tau)\mathrm{d}\tau, \\ S_h = \left(\dfrac{d}{dt} + \lambda_h\right)^4 \displaystyle\int_0^t e_h(\tau)\mathrm{d}\tau, \end{cases} \tag{9}$$

where $e_v(t) = v(t) - v_d(t)$ and $e_h(t) = h(t) - h_d(t)$ are the tracking errors for the velocity channel and the altitude channel, respectively. λ_v and λ_h are the positive constants. The derivatives of Equation (9) can be obtained as

$$\dot{\mathbf{S}} = \begin{cases} \dot{S}_V = \ddot{v} - \ddot{v}_d + 3\lambda_v \ddot{e}_v + 3{\lambda_v}^2 \dot{e}_v + {\lambda_v}^3 e_v, \\ \dot{S}_h = h^{(4)} - h_d^{(4)} + 4\lambda_h \ddot{e}_h + 6{\lambda_h}^2 \ddot{e}_h + 4{\lambda_h}^3 \dot{e}_h + {\lambda_h}^4 e_h. \end{cases} \tag{10}$$

Let $\psi_v = -\ddot{v}_d + 3\lambda_v \ddot{e}_v + 3{\lambda_v}^2 \dot{e}_v + {\lambda_v}^3 e_v$, and $\psi_h = -\mathrm{h}_d^{(4)} + 4\lambda_h \ddot{e}_h + 6{\lambda_h}^2 \ddot{e}_h + 4{\lambda_h}^3 \dot{e}_h + {\lambda_h}^4 e_h$. By introducing the model Equation (6) into Equation (10), we can get

$$\dot{\mathbf{S}} = \begin{cases} \dot{S}_v = F_v + b_{11}U_1 + b_{12}U_2 + \psi_v, \\ \dot{S}_h = F_h + b_{21}U_1 + b_{22}U_2 + \psi_h. \end{cases} \tag{11}$$

(2) Define the sliding mode approaching rate as

$$\dot{\mathbf{S}} = \begin{cases} -\alpha_{v1}|S_v|^{\beta_{v1}} \operatorname{sgn}(S_v) - \alpha_{v2}|S_v|^{\beta_{v2}} \operatorname{sgn}(S_v), \\ -\alpha_{h1}|S_h|^{\beta_{h1}} \operatorname{sgn}(S_h) - \alpha_{h2}|S_h|^{\beta_{h2}} \operatorname{sgn}(\mathrm{S_h}), \end{cases} \tag{12}$$

where $\alpha_{v1} > 0$, $\alpha_{v2} > 0, \alpha_{h1} > 0, \alpha_{h2} > 0, \beta_{v1} > 1, \beta_{h1} > 1, 0 < \beta_{v2} < 1$, and $0 < \beta_{h2} < 1$. When the system state is far away from the sliding mode, $\alpha_{v1}|S_v|^{\beta_{v1}} \operatorname{sgn}(S_v)$ and $\alpha_{h1}|S_h|^{\beta_{h1}} \operatorname{sgn}(S_h)$ play a dominant role, while $\alpha_{v2}|S_v|^{\beta_{v2}} \operatorname{sgn}(S_v)$ and $\alpha_{h2}|S_h|^{\beta_{h2}} \operatorname{sgn}(S_h)$ play a dominant role when the system state is close to the sliding mode. According to Equations (8), (11), and (12), the continuous-time controller can be obtained as follows:

$$\begin{aligned} \mathbf{U} = \begin{bmatrix} U_1 \\ U_2 \end{bmatrix} &= \mathbf{B}^{-1} \begin{bmatrix} -F_v - \psi_v \\ -F_h - \psi_h \end{bmatrix} \\ &+ \mathbf{B}^{-1} \begin{bmatrix} -\alpha_{v1}|S_v|^{\beta_{v1}} \operatorname{sgn}(S_v) - \alpha_{v2}|\mathrm{S_v}|^{\beta_{v2}} \operatorname{sgn}(S_v) - \bar{\mathrm{d}}_1(t) \\ -\alpha_{h1}|S_h|^{\beta_{h1}} \operatorname{sgn}(S_h) - \alpha_{h2}|\mathrm{S_h}|^{\beta_{h2}} \operatorname{sgn}(S_h) - \bar{\mathrm{d}}_2(t) \end{bmatrix}, \end{aligned} \tag{13}$$

where

$$\mathbf{B} = \begin{bmatrix} b_{11} & b_{12} \\ b_{21} & b_{21} \end{bmatrix}. \tag{14}$$

The sliding mode controller can make the system state converge into the neighborhood of the equilibrium zero point quickly, if there are uncertain external disturbances in the system [29]. To ensure the convergence of system state, the observer can be used to compensate the bounded lumped disturbance caused by the system modeling error and bounded external disturbances.

2.3. Design of Traditional Extended State Disturbance Observer. Considering the following third-order system with external disturbances and uncertainties, the state space form is described as

$$\begin{cases} \dot{x}_1 = x_2, \\ \dot{x}_2 = x_3, \\ \dot{x}_3 = f(t, x, w) + B\varnothing(y, u), \\ y = x_1, \end{cases} \tag{15}$$

where $f(t, x, w)$ is the sum of system uncertainties and external disturbances. Equation (15) can be rewritten as follows:

$$\begin{cases} \dot{x}_1 = x_2, \\ \dot{x}_2 = x_3, \\ \dot{x}_3 = x_4 + B\varnothing(y, u), \\ \dot{x}_4 = d, \\ y = x_1, \end{cases} \tag{16}$$

where d is the derivative of the system lumped disturbance. Then, the traditional extended state observer can be designed as follows [25, 26]:

$$\begin{cases} \dot{\bar{x}}_1 = \bar{x}_2 + a_1\omega_0(y - \bar{x}_1), \\ \dot{\bar{x}}_2 = \bar{x}_3 + a_2{\omega_0}^2(y - \bar{x}_1), \\ \dot{\bar{x}}_3 = \bar{x}_4 + \varnothing(y, u) + a_3{\omega_0}^3(y - \bar{x}_1), \\ \dot{\bar{x}}_4 = a_4{\omega_0}^4(y - \bar{x}_1), \end{cases} \tag{17}$$

where $\dot{\bar{x}}_1$, $\dot{\bar{x}}_2$, $\dot{\bar{x}}_3$, and $\dot{\bar{x}}_4$ are observer states, a_1, a_2, a_3, and a_4 are positive real numbers, and ω_0 is the observation bandwidth.

According to the above analyses, the state space model of the velocity channel can be expressed as

$$\begin{cases} \dot{x} = \mathbf{A_1}x + \mathbf{B_1}\varnothing_1(y, u) + \mathbf{w_1}d_1 \\ y = \mathbf{C_1}x \end{cases} \tag{18}$$

where

$$\mathbf{A_1} = \begin{bmatrix} 0 & 1 & 0 & 0 \\ 0 & 0 & 1 & 0 \\ 0 & 0 & 0 & 1 \\ 0 & 0 & 0 & 0 \end{bmatrix},$$

$$\mathbf{B_1} = \begin{bmatrix} 0 \\ 0 \\ 1 \\ 0 \end{bmatrix}, \mathbf{C_1} = \begin{bmatrix} 1 & 0 & 0 & 0 \end{bmatrix},$$

$$\mathbf{w_1} = \begin{bmatrix} 0 \\ 0 \\ 0 \\ 1 \end{bmatrix}, \varnothing_1(y, u) = F_V + b_{11}U_1 + b_{12}U_2. \tag{19}$$

The disturbance observer can be described as

$$\dot{\bar{x}}_v = \mathbf{A_1}\bar{x}_v + \mathbf{B_1}\varnothing_1(y, u) + \mathbf{L_1}(y - \mathbf{C_1}\bar{x}_v), \tag{20}$$

where $\mathbf{L_1} = \begin{bmatrix} a_{v1}\omega_v & a_{v2}{\omega_v}^2 & a_{v3}{\omega_v}^3 & a_{v4}{\omega_v}^4 \end{bmatrix}^T$, $a_{vi} = (4!/\mathrm{i}!(4 - i)!)$, $(i = 1, 2, 3, 4)$, a_{vi} is selected by the bandwidth-based configuration method. More generally, in traditional LESO for any order system, the adjustable parameter only has the observation bandwidth ω_v.

Similarly, the altitude channel can be described as

$$\dot{\bar{x}}_h = \mathbf{A_2}\bar{x}_h + \mathbf{B_2}\varnothing_2(y, u) + \mathbf{L_2}(y - \mathbf{C_2}\bar{x}_h), \tag{21}$$

where

$$\mathbf{A_2} = \begin{bmatrix} 0 & 1 & 0 & 0 & 0 \\ 0 & 0 & 1 & 0 & 0 \\ 0 & 0 & 0 & 1 & 0 \\ 0 & 0 & 0 & 0 & 1 \\ 0 & 0 & 0 & 0 & 0 \end{bmatrix},$$

$$\mathbf{B_2} = \begin{bmatrix} 0 \\ 0 \\ 0 \\ 1 \\ 0 \end{bmatrix},$$

$$\mathbf{C_2} = \begin{bmatrix} 1 \\ 0 \\ 0 \\ 0 \\ 0 \end{bmatrix}^{\mathrm{T}},$$

$$\varnothing_2(\mathrm{y}, u) = F_h + b_{21}U_1 + b_{22}U_2,$$

$$\mathbf{L_2} = \begin{bmatrix} a_{h1}\omega_h & a_{h2}{\omega_h}^2 & a_{h3}{\omega_h}^3 & a_{h4}{\omega_h}^4 & a_{h5}{\omega_h}^5 \end{bmatrix}^T,$$

$$\mathrm{a_{hi}} = \frac{5!}{\mathrm{i}!(5 - \mathrm{i})!}, (\mathrm{i} = 1, 2, 3, 4, 5), \tag{22}$$

and the adjustable parameter only has the observation bandwidth ω_h.

Combined Equation (20) with Equation (21), the aircraft disturbance observer can be described as

$$\dot{\bar{x}} = \mathbf{A}\bar{x} + \mathbf{B}\varnothing(\mathbf{y}, \mathbf{u}) + \mathbf{L}(y - \mathbf{C}\bar{x}), \tag{23}$$

where

$$
\mathbf{A} = \begin{bmatrix}
0 & 1 & 0 & 0 & & 0 & 0 & 0 & 0 & 0 \\
0 & 0 & 1 & 0 & & 0 & 0 & 0 & 0 & 0 \\
0 & 0 & 0 & 1 & & 0 & 0 & 0 & 0 & 0 \\
0 & 0 & 0 & 0 & & 0 & 0 & 0 & 0 & 0 \\
0 & 0 & 0 & 0 & & 0 & 1 & 0 & 0 & 0 \\
0 & 0 & 0 & 0 & & 0 & 0 & 1 & 0 & 0 \\
0 & 0 & 0 & 0 & & 0 & 0 & 0 & 1 & 0 \\
0 & 0 & 0 & 0 & & 0 & 0 & 0 & 0 & 1 \\
0 & 0 & 0 & 0 & & 0 & 0 & 0 & 0 & 0
\end{bmatrix},
$$

$$
\mathbf{B} = \begin{bmatrix}
0 & 0 \\
0 & 0 \\
1 & 0 \\
0 & 0 \\
0 & 0 \\
0 & 0 \\
0 & 0 \\
0 & 1 \\
0 & 0
\end{bmatrix},
$$

$$
\mathbf{C} = \begin{bmatrix}
1 & 0 \\
0 & 0 \\
0 & 0 \\
0 & 0 \\
0 & 1 \\
0 & 0 \\
0 & 0 \\
0 & 0 \\
0 & 0
\end{bmatrix}^{\mathrm{T}},
\tag{24}
$$

$$
\varnothing(\mathbf{y}, \mathbf{u}) = \begin{bmatrix} F_V + b_{11}U_1 + b_{12}U_2 \\ F_h + b_{21}U_1 + b_{22}U_2 \end{bmatrix},
$$

$$
\mathbf{L} = \begin{bmatrix}
a_{v1}\omega_v & a_{v2}{\omega_v}^2 & a_{v3}{\omega_v}^3 & a_{v4}{\omega_v}^4 & 0 & 0 & 0 & 0 & 0 \\
0 & 0 & 0 & 0 & a_{h1}\omega_h & a_{h2}{\omega_h}^2 & a_{h3}{\omega_h}^3 & a_{h4}{\omega_h}^4 & a_{h5}{\omega_h}^5
\end{bmatrix}^T.
$$

3. Proposed High-Order Linear Extended State Observer

3.1. Design of High-Order Linear Extended State Observer. For the sake of generality, the following m-th order system with external disturbances and uncertainties are considered. The state space form can be described as

$$
\begin{cases}
\dot{\mathrm{x}}_1 = x_2, \\
\dot{\mathrm{x}}_2 = x_3, \\
\quad \vdots \\
\dot{\mathrm{x}}_m = f(t, x, w) + \mathrm{B}\varnothing(y, u) \\
\dot{\mathrm{x}}_{m+1} = \dot{f}(t, x, w), \\
y = x_1,
\end{cases}
\tag{25}
$$

where its extended first-order state observer (traditional LESO) is given as

$$\begin{cases} \dot{\bar{x}}_1 = \bar{x}_2 + a_1\omega_0(y - \bar{x}_1), \\ \dot{\bar{x}}_2 = \bar{x}_3 + a_2{\omega_0}^2(y - \bar{x}_1), \\ \quad\vdots \\ \dot{\bar{x}}_m = \bar{x}_{m+1} + \mathrm{B}\varnothing(y, u) + a_m{\omega_0}^m(y - \bar{x}_1), \\ \dot{\bar{x}}_{m+1} = a_{m+1}{\omega_0}^{m+1}(y - \bar{x}_1). \end{cases} \tag{26}$$

The following hypothesis proposed in [22] is given as

Assumption 3. The derivatives of the lumped disturbance $f(t, x, w)$ of the system exist and are bounded as $|d^n f(t, x, w)/dt^n| \le \theta$.

Accordingly, the form of state equation and extended $(n+1)$-th order state observer can be presented as

$$\begin{cases} \dot{x}_1 = x_2, \\ \dot{x}_2 = x_3, \\ \quad\vdots \\ \dot{x}_m = f(t, x, w) + \mathrm{B}\varnothing(y, u), \\ \dot{x}_{m+1} = x_{m+2}, \\ \quad\vdots \\ \dot{x}_{m+n} = x_{m+n+1,} \\ y = x_1. \end{cases} \tag{27}$$

$$\begin{cases} \dot{\bar{x}}_1 = \bar{x}_2 + a_1\omega_0(y - \bar{x}_1), \\ \dot{\bar{x}}_2 = \bar{x}_3 + a_2{\omega_0}^2(y - \bar{x}_1), \\ \quad\vdots \\ \dot{\bar{x}}_m = \bar{x}_{m+1} + \mathrm{B}\varnothing(y, u) + a_m{\omega_0}^m(y - \bar{x}_1), \\ \dot{\bar{x}}_{m+1} = \bar{x}_{m+2} + a_{m+1}{\omega_0}^{m+1}(y - \bar{x}_1), \\ \dot{\bar{x}}_{m+2} = \bar{x}_{m+3} + a_{m+2}{\omega_0}^{m+2}(y - \bar{x}_1), \\ \quad\vdots \\ \dot{\bar{x}}_{m+n} = \bar{x}_{m+n+1} + a_{m+n}{\omega_0}^{m+n}(y - \bar{x}_1), \\ \dot{\bar{x}}_{m+n+1} = a_{m+n+1}{\omega_0}^{m+n+1}(y - \bar{x}_1), \end{cases} \tag{28}$$

where x_{m+1} is the lumped disturbance $f(t, x, w)$, x_{m+2}, x_{m+3}, $\cdots$, x_{m+n+1} are the first, second, $\cdots$, and n-th order derivatives of the lumped disturbance, respectively. $\dot{\bar{x}}_{m+1}$ is the estimate of lumped disturbance $f(t, x, w)$, and $\bar{x}_{m+2}$, $\bar{x}_{m+2}$, $\cdots$, $\bar{x}_{m+n+1}$ are severally the estimates of the first, second, $\cdots$, and n-th order derivatives of the lumped disturbance. The parameter $a_i = (m+n+1)!/i!(m+n+1-i)!\,(\mathrm{i} = 1, 2, \cdots, \mathrm{m}+n+1)$ is selected by the bandwidth-based configuration method, and ω_0 is the observation bandwidth, and $n = 0$ indicates the traditional LESO.

3.2. Convergence Analysis. In this section, the convergence analysis is presented. First, the definition of the expansion of $(\mathrm{n}+1)$-th order state observer for the m-th order system is given below

$$\begin{aligned} &e_i(t) = x_i(t) - \bar{x}_i(t), \\ &\eta_{\mathrm{i}}(t) = \frac{e_i(\varepsilon t)}{\varepsilon^{m+n+1-i}}, (i = 1, 2, \cdots, \mathrm{m}+n+1), \end{aligned} \tag{29}$$

$$\begin{aligned} \boldsymbol{\eta} = [&\eta_1(t), \quad \eta_2(t), \quad \eta_3(t), \cdots, \eta_m(t), \quad \eta_{m+1}(t), \\ &\cdots, \eta_{m+n}(t), \eta_{m+n+1}(t)]^T. \end{aligned} \tag{30}$$

The differential form of $\eta_{\mathrm{i}}(t)$ can be described as

$$\begin{cases} \dot{\eta}_1(t) = \eta_2 - g_1(\eta_1(t)), \\ \dot{\eta}_2(t) = \eta_3 - g_2(\eta_1(t)), \\ \quad\vdots \\ \dot{\eta}_{m+n}(t) = \eta_{m+n+1} - g_{m+\mathrm{n}}(\eta_1(t)), \\ \dot{\eta}_{m+n+1}(t) = -g_{m+n+1}(\omega_1(t)) + \varepsilon\Delta(t), \end{cases}$$

$$\begin{cases} \eta_1(0) = \dfrac{e_1(0)}{\varepsilon^{m+n}}, \\ \eta_2(0) = \dfrac{e_2(0)}{\varepsilon^{m+n-1}}, \\ \quad\vdots \\ \eta_{m+n}(0) = \dfrac{e_{m+n}(0)}{\varepsilon}, \\ \eta_{m+n+1}(0) = e_{m+n+1}(0), \end{cases} \tag{31}$$

where $1/\varepsilon$ is the observation bandwidth.

For clear illustration, the following hypothesis and theorem proposed in [22] are provided first.

Assumption 4. There are certain constants of $\lambda_{\mathrm{i}}(i = 1, 2, 3, 4)$, k, and the positive definite continuous differentiable functions V and W: $\mathbb{R}^{m+n+1} \longrightarrow \mathbb{R}$, which make

$$\begin{cases} \lambda_1\|\omega\|^2 \le V(\omega) \le \lambda_2\|\omega\|^2, \\ \lambda_3\|\omega\|^2 \le W(\omega) \le \lambda_4\|\omega\|^2, \\ \displaystyle\sum_{\mathrm{i}=1}^{m+n+1} \frac{\partial V}{\partial \eta_i}(\eta_{i+1} - g_i(\eta_1)) - \frac{\partial V}{\partial \eta_{m+n+1}} g_{m+n+1}(\eta_1(t)) \le -W(\eta), \left|\dfrac{\partial V}{\partial \eta_{m+n+1}}\right| \le k\|\eta\|, \end{cases} \tag{32}$$

where $\|\bullet\|$ is the Euclid norm.

Theorem 5. *If Assumption 3 and Assumption 4 are satisfied, then for the system Equation (28), the following conclusion is true.*

$$SUP\,|x_i(t)-\bar{x}_i(t)| \le O\left(\varepsilon^{m+n+2-i}\right), \forall t \in [t_u, \infty) 0 < \varepsilon < 1. \tag{33}$$

According to Assumption 3 and Assumption 4, it can be concluded that

$$\begin{aligned}\frac{d}{dt}V(\omega(t)) &= \sum_{i=1}^{m+n+1}\frac{\partial V}{\partial \eta_i}(\eta_{i+1}-g_i(\eta_1)) - \frac{\partial V}{\partial \eta_{m+n+1}}g_{m+n+1}(\eta_1(t)) \\ &\quad + \frac{\partial V}{\partial \eta_{m+n+1}}\varepsilon\Delta(t) \le -W(\eta)+\varepsilon\theta k\|\eta\| \\ &\le -\frac{\lambda_3}{\lambda_2}V(\eta) + \frac{\sqrt{\lambda_1}}{\lambda_1}\varepsilon\theta k\sqrt{V(\eta)}.\end{aligned} \tag{34}$$

Considering the relationship between $V(\eta)$ and $\sqrt{V(\eta)}$, there is

$$\frac{d}{dt}\sqrt{V(\eta(t))} \le -\frac{\lambda_3}{\lambda_2}\sqrt{V(\eta(t))} + \frac{\sqrt{\lambda_1}}{2\lambda_1}\varepsilon\theta k. \tag{35}$$

Then, according to Gronwall-Bellman inequality, we can obtain

$$\|\eta(t)\| \le \sqrt{\frac{V(\eta(t))}{\lambda_1}} \le \frac{\sqrt{\lambda_1 V(\eta(0))}}{\lambda_1}e^{-\frac{\lambda_3(t-t_0)}{2\varepsilon\lambda_2}} + \frac{\varepsilon\theta k}{2\lambda_1}\int_0^t e^{-\frac{\lambda_3}{2\lambda_2}(t-t_0-s)}ds. \tag{36}$$

Finally, the inequality of $e_i(t)$ can be concluded from the relationship of $\eta(t)$ and $e(t)$ as

$$\begin{aligned}|e_i(t)| &= \eta_i\left(\frac{t}{\varepsilon}\right)\varepsilon^{m+n+1-i} \le \left\|\eta\left(\frac{t}{\varepsilon}\right)\right\|\varepsilon^{m+n+1-i} \\ &\le \varepsilon^{m+n+1-i}\left[\frac{\sqrt{\lambda_1 V(\eta(0))}}{\lambda_1}e^{-\frac{\lambda_3(t-t_0)}{2\varepsilon\lambda_2}} + \frac{\varepsilon\theta k}{2\lambda_1}\int_{\frac{t_0}{\varepsilon}}^{\frac{t}{\varepsilon}} e^{-\frac{\lambda_3}{2\lambda_2}\left(\frac{(t-t_0)}{\varepsilon}-s\right)}ds\right] \\ &\le O\left(\varepsilon^{m+n+2-i}\right), \forall t \in [t_u, \infty),\end{aligned} \tag{37}$$

where $t_u = \max\{t_0 - 2\lambda_2/\lambda_3(m+n+1)\varepsilon\ln\varepsilon, t_0\}$.

Accordingly, when the perturbation parameters are small enough, the estimated state of the system Equation (28) is sufficiently close to the state of the system Equation (27). The estimation error converges to $O(\varepsilon^{m+n+2-i})$ and decreases with the increase of the expansion order.

3.3. Stability Analysis

Theorem 6. *For the nonlinear dynamic model of NSV control system show in Equation (1), the continuous time controller of Equation (13) is chosen as the disturbance compensation controller, considering the uncertainty and external disturbance. The system is asymptotically stable when the following conditions are satisfied.*

$$\begin{cases} |S_v| \le \min\left\{\left(\dfrac{D_v}{\alpha_{v2}}\right)^{1/\beta_{v2}}, \left(\dfrac{D_v}{\alpha_{v1}}\right)^{1/\beta_{v1}}\right\}, \\ |S_h| \le \min\left\{\left(\dfrac{D_h}{\alpha_{h2}}\right)^{1/\beta_{h2}}, \left(\dfrac{D_h}{\alpha_{h1}}\right)^{1/\beta_{h1}}\right\}. \end{cases} \tag{38}$$

The Lyapunov function is defined as

$$L = \frac{1}{2}S^TS, \tag{39}$$

$$\begin{aligned}\dot{L} = S^T\dot{S} &= S_v\dot{S}_v + S_h\dot{S}_h = -\alpha_{v1}|S_v|^{\beta_{v1}}\,\mathrm{sgn}\,(S_v) - \alpha_{v2}|S_v|^{\beta_{v2}}\,\mathrm{sgn}\,(S_v) \\ &\quad - \alpha_{h1}|S_h|^{\beta_{h1}}\,\mathrm{sgn}\,(S_h) - \alpha_{h2}|S_h|^{\beta_{h2}}\,\mathrm{sgn}\,(S_h) \\ &\quad + S_v\left[b_{11}\tilde{d}_1(t) + b_{12}\tilde{d}_2(t)\right] + S_h\left[b_{21}\tilde{d}_1(t) + b_{22}\tilde{d}_2(t)\right] \\ &\le -\alpha_{v1}|S_v|^{\beta_{v1}+1} - \alpha_{v2}|S_v|^{\beta_{v2}+1} - \alpha_{h1}|S_h|^{\beta_{h1}+1} - \alpha_{h2}|S_h|^{\beta_{h2}+1} \\ &\quad + |S_v||D_v| + |S_h||D_h|,\end{aligned} \tag{40}$$

where $\tilde{d}_i(t) = d_i(t) - \bar{d}_i(t)$, $|\tilde{d}_i(t)| \le k$, $(i = 1, 2)$, $d_i(t)$ is the lumped disturbance, $\bar{d}_i(t)$ is the estimate of lumped disturbance, $\alpha_{v1} > 0$, $\alpha_{v2} > 0$, $\alpha_{h1} > 0$, $\alpha_{h2} > 0$,

$$\begin{cases} b_{11}\tilde{d}_1(t) + b_{12}\tilde{d}_2(t) \le (b_{11}+b_{12})k = |D_v|, \\ b_{21}\tilde{d}_1(t) + b_{22}\tilde{d}_2(t) \le (b_{21}+b_{22})k = |D_h|. \end{cases} \tag{41}$$

The inequality (40) can be described as the following two forms:

$$\begin{aligned}\dot{L} &\le -|S_v|\left(\alpha_{v2}|S_v|^{\beta_{v2}} - |D_v|\right) - |S_h|\left(\alpha_{h2}|S_h|^{\beta_{h2}} - |D_h|\right) \\ &\quad - \alpha_{v1}|S_v|^{\beta_{v1}+1} - \alpha_{h1}|S_h|^{\beta_{h1}+1},\end{aligned} \tag{42}$$

$$\begin{aligned}\dot{L} &\le -|S_v|\left(\alpha_{v1}|S_v|^{\beta_{v1}} - |D_v|\right) - |S_h|\left(\alpha_{h1}|S_h|^{\beta_{h1}} - |D_h|\right) \\ &\quad - \alpha_{v2}|S_v|^{\beta_{v2}+1} - \alpha_{h2}|S_h|^{\beta_{h2}+1}.\end{aligned} \tag{43}$$

From inequality (42), we can obtain

$$\dot{L} \le -\alpha_{v1}|S_v|^{\beta_{v1}+1} - \alpha_{h1}|S_h|^{\beta_{h1}+1} \le 0, \tag{44}$$

when

$$\begin{cases} |S_v| \ge \left(\dfrac{D_v}{\alpha_{v2}}\right)^{1/\beta_{v2}}, \\ |S_h| \ge \left(\dfrac{D_h}{\alpha_{h2}}\right)^{1/\beta_{h2}}. \end{cases} \tag{45}$$

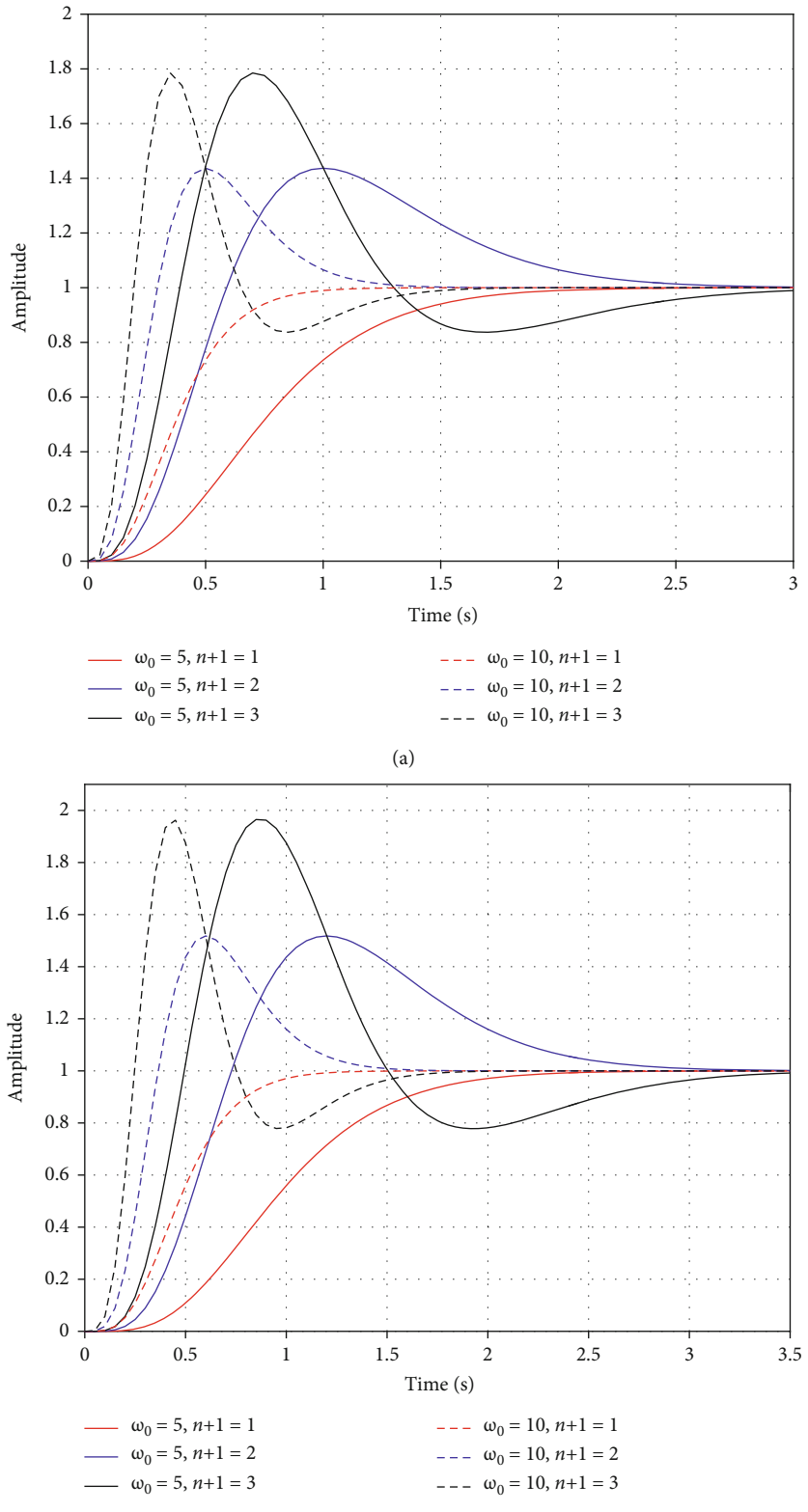

Figure 1: Step response of high-order LESO disturbance estimates: (a) system order is 3; (b) system order is 4.

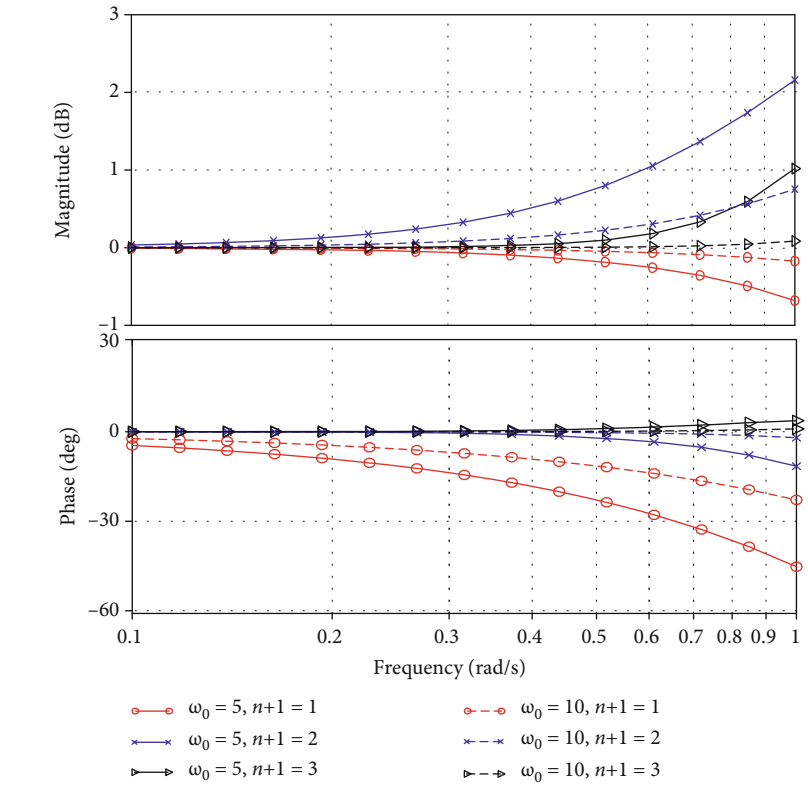

(a)

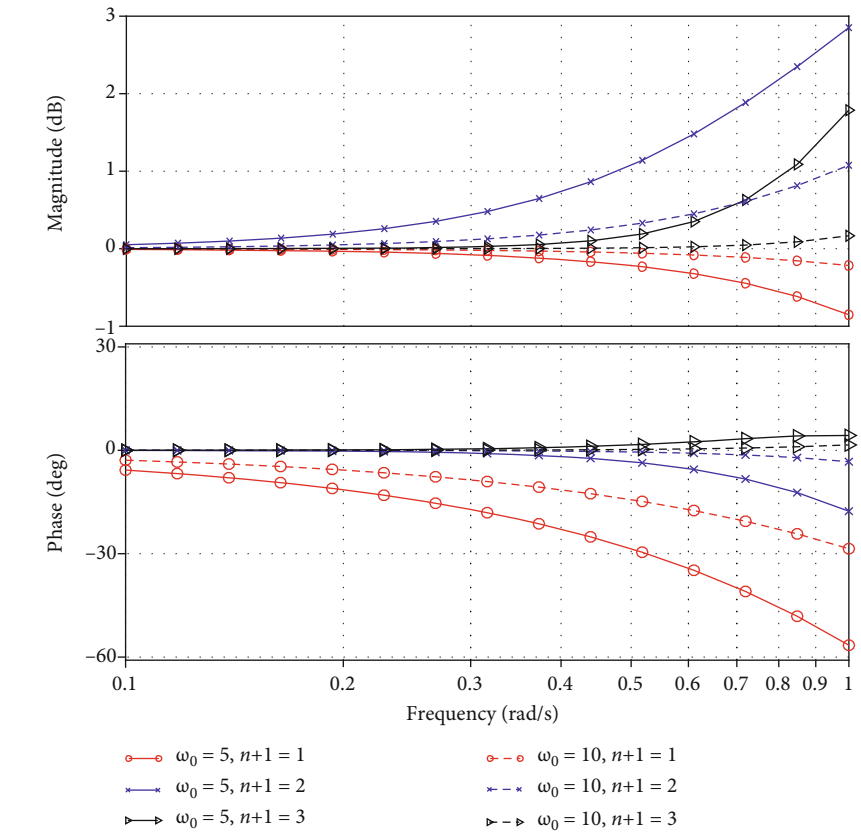

(b)

Figure 2: Low-frequency characteristics of high-order LESO disturbance estimates: (a) system order is 3; (b) system order is 4.

Table 1: Magnitude errors of high-order LESO in the low-frequency band.

System order	Expansion order	Observation bandwidth	Magnitude errors at 0.2 rad/s (dB)	Magnitude errors at 0.4 rad/s (dB)	Magnitude errors at 0.8 rad/s (dB)
3	1	5	-0.0277	-0.111	-0.44
3	2	5	0.135	0.506	1.6
3	3	5	0.00232	0.0361	0.485
3	1	10	-0.00695	-0.0277	-0.111
3	2	10	0.0346	0.135	0.506
3	3	10	0.000148	0.00232	0.0361
4	1	5	-0.0347	-0.139	-0.55
4	2	5	0.201	0.736	2.18
4	3	5	0.00461	0.071	0.902
4	1	10	-0.0087	-0.0348	-0.139
4	2	10	0.0516	0.202	0.735
4	3	10	0.000292	0.00462	0.0711

Table 2: Phase errors of high-order LESO in the low-frequency band.

System order	Expansion order	Observation bandwidth	Phase errors at 0.2 rad/s (deg)	Phase errors at 0.4 rad/s (deg)	Phase errors at 0.8 rad/s (deg)
3	1	5	-9.14	-18.3	-36.4
3	2	5	-0.143	-1.07	-6.81
3	3	5	0.0715	0.526	2.77
3	1	10	-4.58	-9.14	-18.3
3	2	10	-0.0182	-0.143	-1.07
3	3	10	0.00911	0.0715	0.526
4	1	5	-11.4	-22.9	-45.5
4	2	5	-0.248	-1.81	-10.07
4	3	5	0.125	0.884	3.93
4	1	10	-5.72	-11.5	-22.9
4	2	10	-0.0317	-0.249	-1.81
4	3	10	0.0159	0.124	0.886

From inequality (43), we can obtain

$$\dot{L} \le -\alpha_{v2}|S_v|^{\beta_{v2}+1} - \alpha_{h2}|S_h|^{\beta_{h2}+1} \le 0, \tag{46}$$

when

$$\begin{cases} |S_v| \ge \left(\dfrac{D_v}{\alpha_{v1}}\right)^{1/\beta_{v1}}, \\ |S_h| \ge \left(\dfrac{D_h}{\alpha_{h1}}\right)^{1/\beta_{h1}}. \end{cases} \tag{47}$$

In conclusion, the states $|S_v|$ and $|S_h|$ converge to the following regions in the finite time.

$$\begin{cases} |S_v| \le \min\left\{\left(\dfrac{D_v}{\alpha_{v2}}\right)^{1/\beta_{v2}}, \left(\dfrac{D_v}{\alpha_{v1}}\right)^{1/\beta_{v1}}\right\}, \\ |S_h| \le \min\left\{\left(\dfrac{D_h}{\alpha_{h2}}\right)^{1/\beta_{h2}}, \left(\dfrac{D_h}{\alpha_{h1}}\right)^{1/\beta_{h1}}\right\}. \end{cases} \tag{48}$$

4. Results and Discussion

In this simulation parts, we first analyze the influence of the extended order and observation bandwidth on the observer performance; then, we further verify the performance of proposed observer in the NSV control system.

4.1. Parameter Analysis. According to Equation (27) and Equation (28), we can deduce the transfer function from lumped disturbances to disturbance estimate and disturbance estimate error as follows:

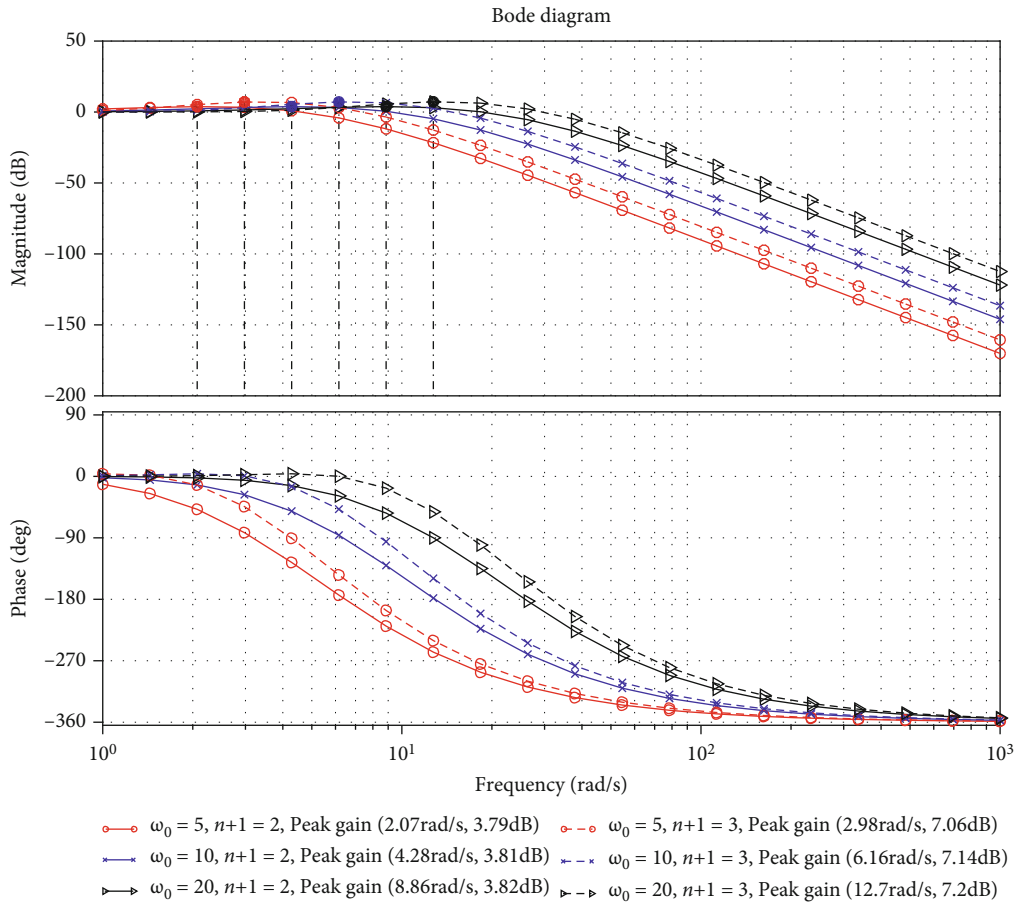

(a)

Figure 3: Continued.

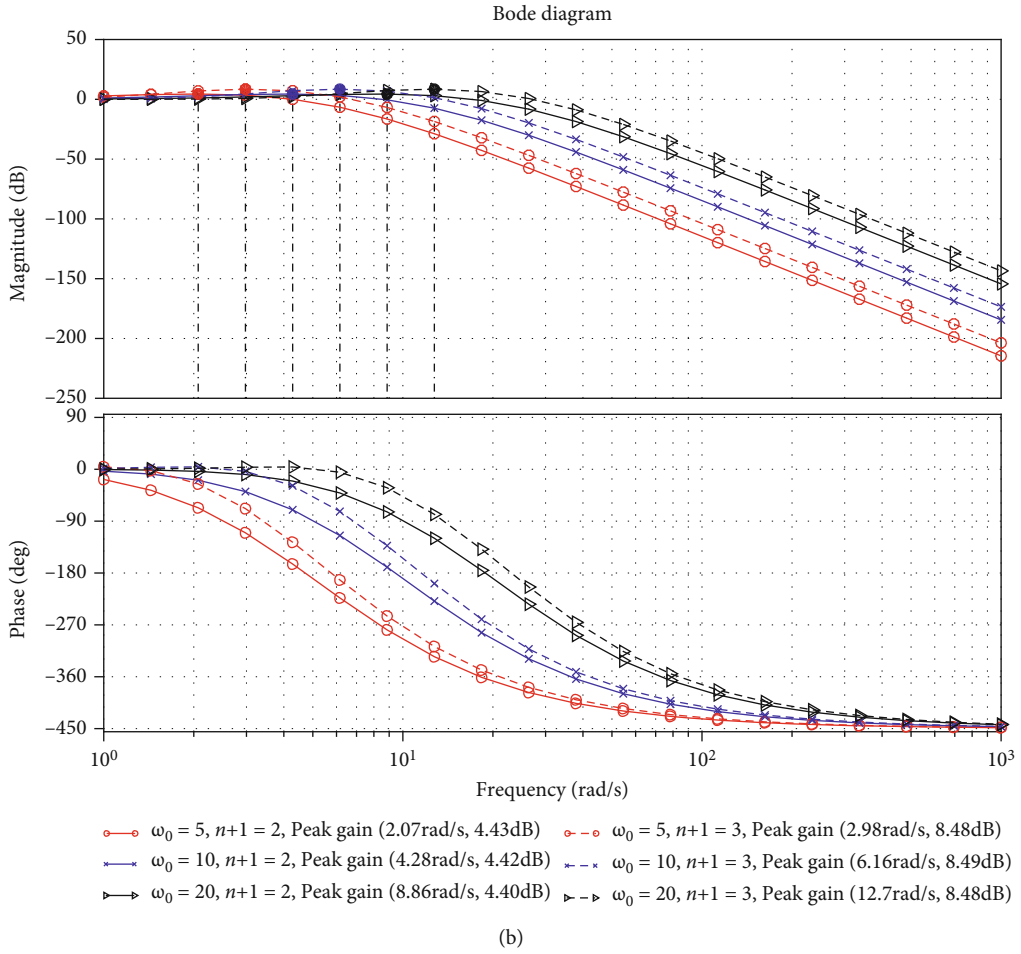

(b)

Figure 3: Intermediate-frequency and high-frequency characteristics of high-order LESO disturbance estimates: (a) system order is 3; (b) system order is 4.

$$\frac{\bar{f}(s)}{f(s)} = \frac{(s+\omega_0)^{m+n+1} - s^{m+n+1} - \sum_{i=1}^{m} a_i \omega_0{}^i s^{m+n+1-i}}{(s+\omega_0)^{m+n+1}}, \quad (49)$$

$$\frac{\bar{Q}(s)}{f(s)} = \frac{s^{m+n+1} + \sum_{i=1}^{m} a_i \omega_0{}^i s^{m+n+1-i}}{(s+\omega_0)^{m+n+1}}, \quad (50)$$

where $\bar{Q}(s)$ is the lumped disturbance estimate error, m is the system order, $n+1$ is the expansion order, ω_0 is the observation bandwidth, and $a_i = (m+n+1)!/i!(m+n+1-i)!(i = 1, 2, \cdots, m+n+1)$.

Furthermore, the performance analysis of the expansion order and the observation bandwidth is also provided in the time domain and the frequency domain over the third-order velocity channel and the fourth-order altitude channel, respectively. According to Equation (49), the high-order LESO has the following characteristics.

As can be seen from Figure 1, when the observation bandwidth is a constant, the higher the expansion order, the faster the response speed, but the overshoot will increase. When the expansion order is a constant, the bigger the observation bandwidth, the faster the response speed, and the overshoot remains unchanged. It can be seen from the overall effect that the higher the system order, the greater the overshoot. Therefore, it is particularly important to choose the appropriate observation bandwidth and expansion order.

Figure 2 shows the low-frequency characteristics of high-order LESO lumped disturbance estimates, where the frequency range is $[0.1, 1]$. Moreover, the reference frequencies are selected as 0.2, 0.4, and 0.8, respectively. The amplitude frequency characteristics and phase frequency characteristics are shown in Tables 1 and 2, respectively. Compared with the traditional LESO, when the expansion order is $n+1=2$, the amplitude errors increase slightly, but the phase errors decrease greatly. When the expansion order is $n+1=3$, the amplitude errors and phase errors are smaller than $n+1=1$ and $n+1=2$. When the expansion order is a constant, the larger the observation bandwidth, the smaller of magnitude errors and phase errors. It has been shown in Tables 1 and 2 that the estimation error is also related to the system order. Both of the magnitude errors and the phase errors will increase as the system order becomes higher. Generally, in the low-frequency

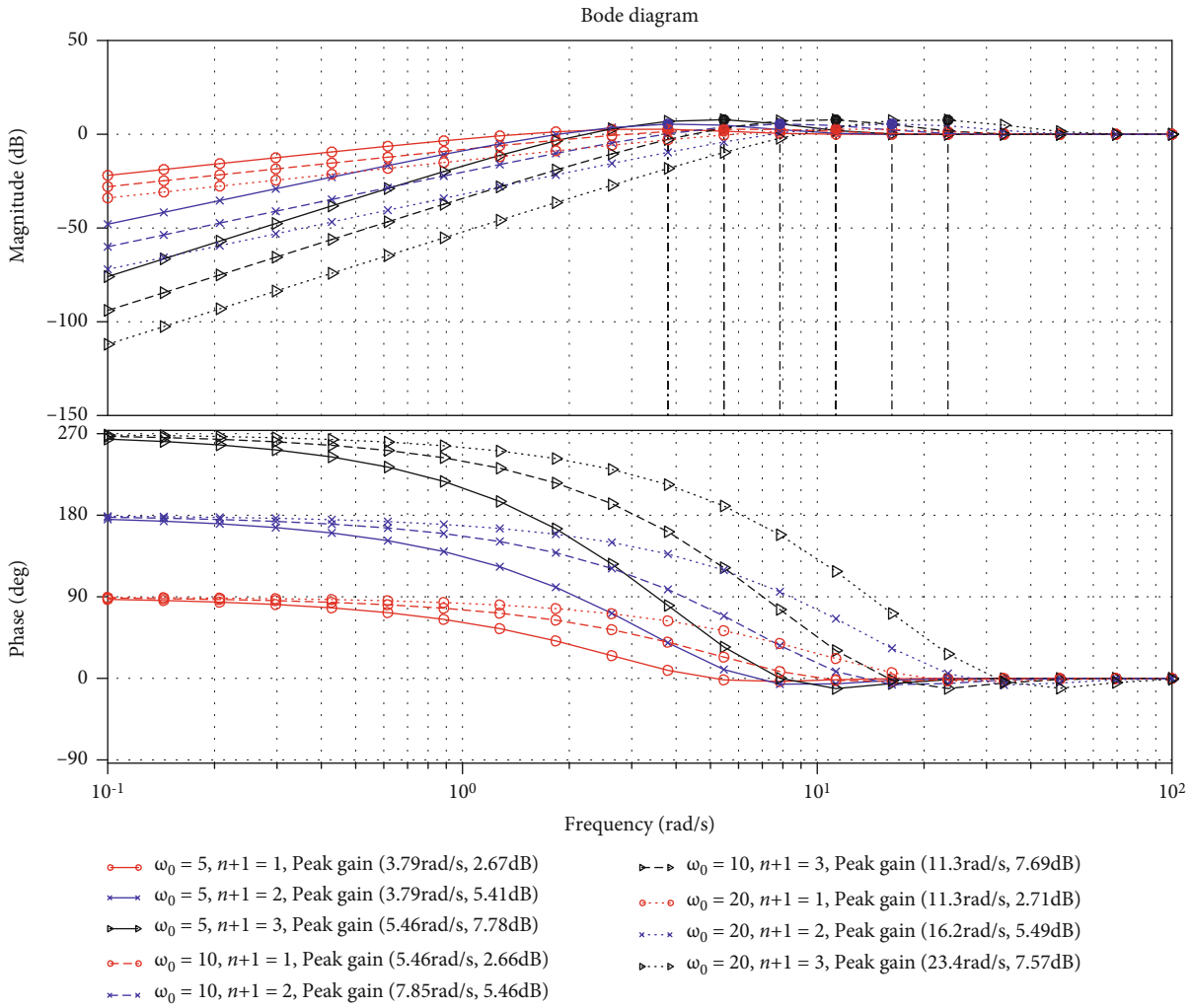

(a)

Figure 4: Continued.

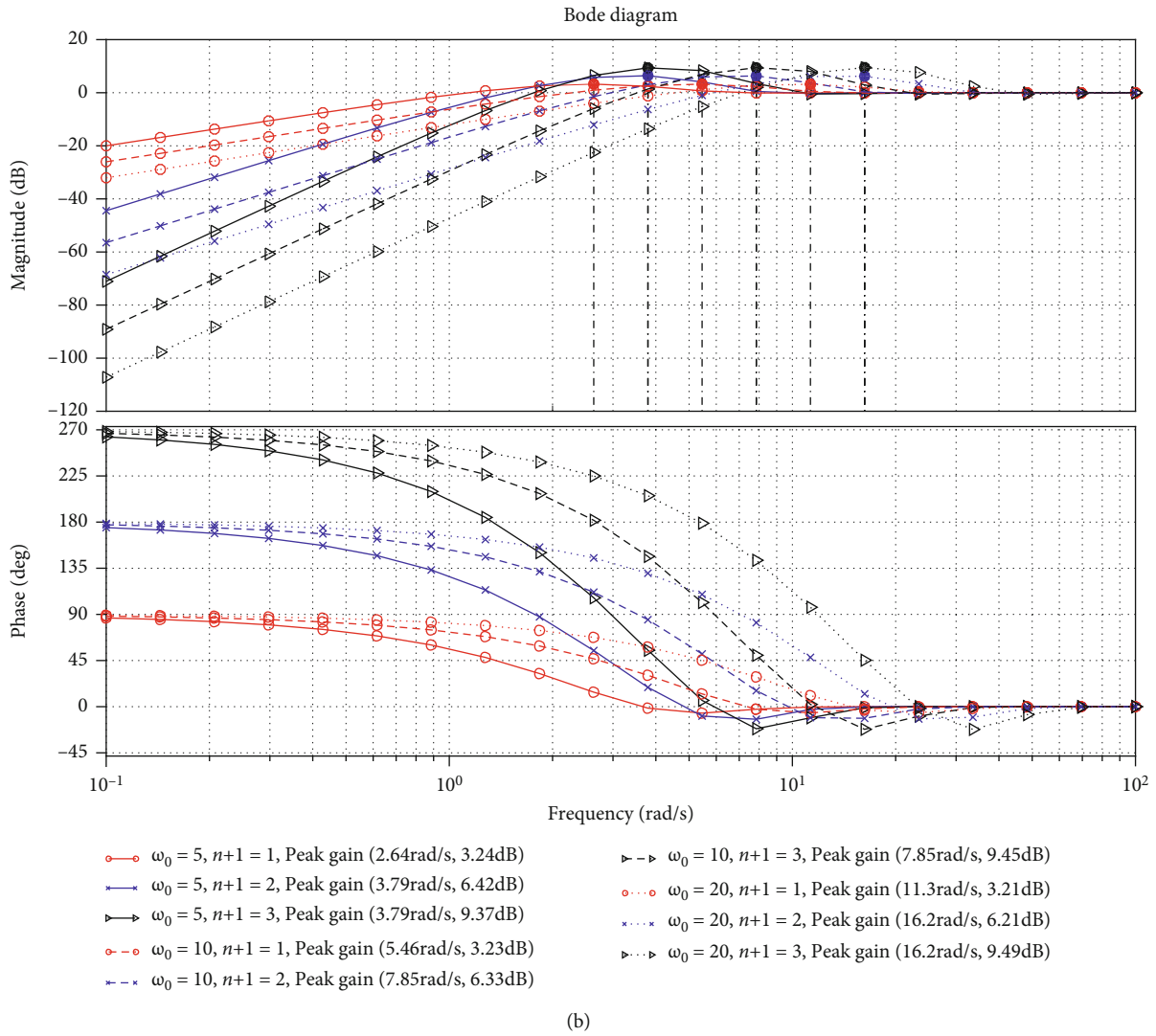

(b)

Figure 4: High-order LESO disturbance suppression frequency response: (a) system order is 3; (b) system order is 4.

band, the estimation errors of high-order LESO are smaller than those of the traditional LESO.

According to Equation (50), it can be seen from Figures 3 and 4 that, at the same observer bandwidth, increasing the order of the extended state can significantly enhance the disturbance suppression in the low-frequency band, which is conducive to better tracking the system state and disturbance. However, in the intermediate-frequency band, the high-order LESO has larger peak amplitudes, which would lead to bigger overshoots or oscillations of the step response, which is not helpful to the system stability. Furthermore, the observation bandwidth only affects the rapidity of high-order LESO, and the overshoot is not affected by the bandwidth, but only related to the expansion order.

In general, both increasing the observation bandwidth and the expansion order can improve the low-frequency performance of observer. However, the higher the expansion order, the bigger the peak amplitude of intermediate frequency, which is prone to lead a larger overshoot and even oscillation; the lager the observation bandwidth, the worse the intermediate-frequency and high-frequency characteristics. Furthermore, the higher the order of the system, the greater the estimation errors. Therefore, for high-order system, we use high-order LESO by choosing appropriate observation bandwidth and expansion order, which has better low-frequency characteristics than traditional LESO.

4.2. Numerical Simulations. In order to verify the effectiveness of the proposed method, the mathematical model of the NSV is built on the MATLAB/Simulink platform, and the designed controller is also simulated and verified with MATLAB.

In this paper, based on the flight conditions of NSV cruise state, the uncertain parameters are adopted as additional variables. The main parameters are set as follows: $m_0 = 50200$ kg, $v_0 = 4590$ m/s, $h_0 = 33528$ m, $s_0 = 369$ m^2, $c_0 = 28$ m, and $I_{y0} = 8466900$ kg•m^2. The parametric uncertainty is defined as

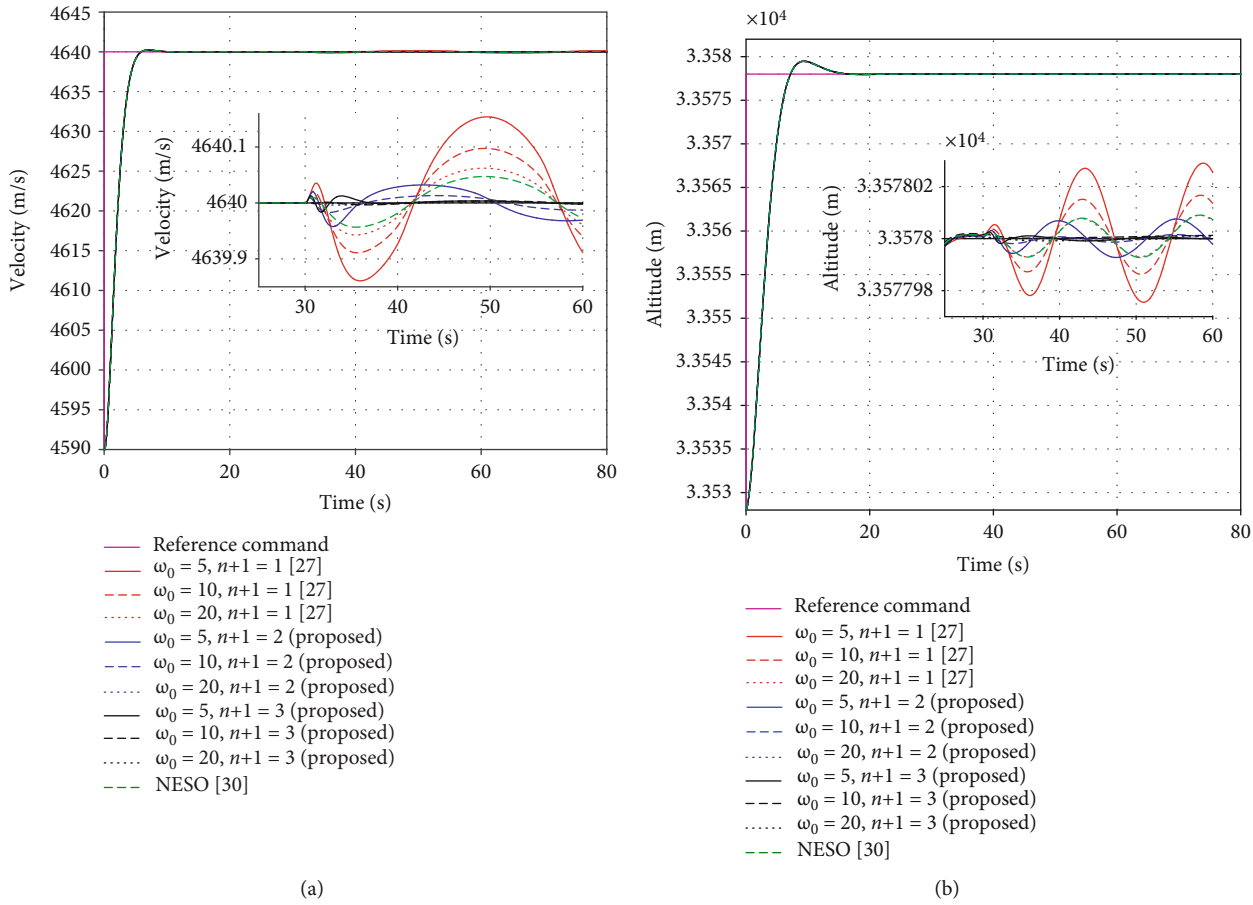

Figure 5: The response curves of NSV: (a) velocity channel; (b) altitude channel.

$$\begin{cases} m = m_0(1+\Delta m),\ |\Delta m| \le 0.03, \\ I_y = I_{y0}(1+\Delta I_y),\ |\Delta I_y| \le 0.02, \\ s = s_0(1+\Delta s),\ |\Delta s| \le 0.01, \\ c = c_0(1+\Delta c),\ |\Delta c| \le 0.03, \\ c_e = c_{e0}(1+\Delta c_e),\ |\Delta c_e| \le 0.02, \\ \rho = \rho_0(1+\Delta\rho),\ |\Delta\rho| \le 0.03. \end{cases} \tag{51}$$

The expansion orders of $n+1=1$, $n+1=2$, and $n+1=3$ in addition with observation bandwidth of $\omega_0 = 5$, $\omega_0 = 10$, and $\omega_0 = 20$ are adopted in the simulations, respectively. Thereinto, $n+1=1$ indicates the traditional LESO, while $n+1=2$ and $n+1=3$ are the recommended LESO in this paper. Under the premise of system stability, the parameters of controller and observer are basically unchanged. Moreover, due to the coupling between the velocity and altitude channels, the observer output needs to be decoupled. The step signal for velocity channel and altitude channel are given as 50 m/s and 50 m, respectively. The external disturbance $d_1(t) = 0.02\sin(0.4t)$ and $d_2(t) = 0.04\sin(0.2t)$ are introduced in the 30th second.

The simulation results are shown in Figures 5–8, where the curves with parameter of $n+1=1$ indicate the algorithm in [27], the others with parameter of $n+1=2$ and $n+1=3$ represent our proposed algorithm, and the compared nonlinear extended state observer (NESO) is proposed in [30]. Figure 5 shows the time response of compared NSV observers over the velocity channel and altitude channel. It can be seen in Figure 5 that both the controllers with LESO and NESO with appropriate parameters can make the system stable. As to the overall effect, the steady-state accuracy of the proposed high-order LESO is obviously better than traditional LESO. When the expansion order parameter is selected as $n+1=2$, the steady-state accuracy of proposed observer is similar to that of NESO. Furthermore, when the expansion order parameter is selected as $n+1=3$, the steady-state accuracy of proposed observer is better than NESO. Figure 6 shows the time responses of the observer errors over the velocity channel and altitude channel, where the disturbance estimation errors of the proposed high-order LESO are obviously smaller than traditional LESO and NESO. Figure 7 shows the time responses of the actuator on throttle setting and elevator deflection. It can be concluded from Figure 7 that with the increase of the order and observer bandwidth, the control signal will generate peak amplitude and high-frequency oscillations, which are deleterious to the actuator. However, the curve of NESO is smoother than LESO. The higher the system order and the lager the observer

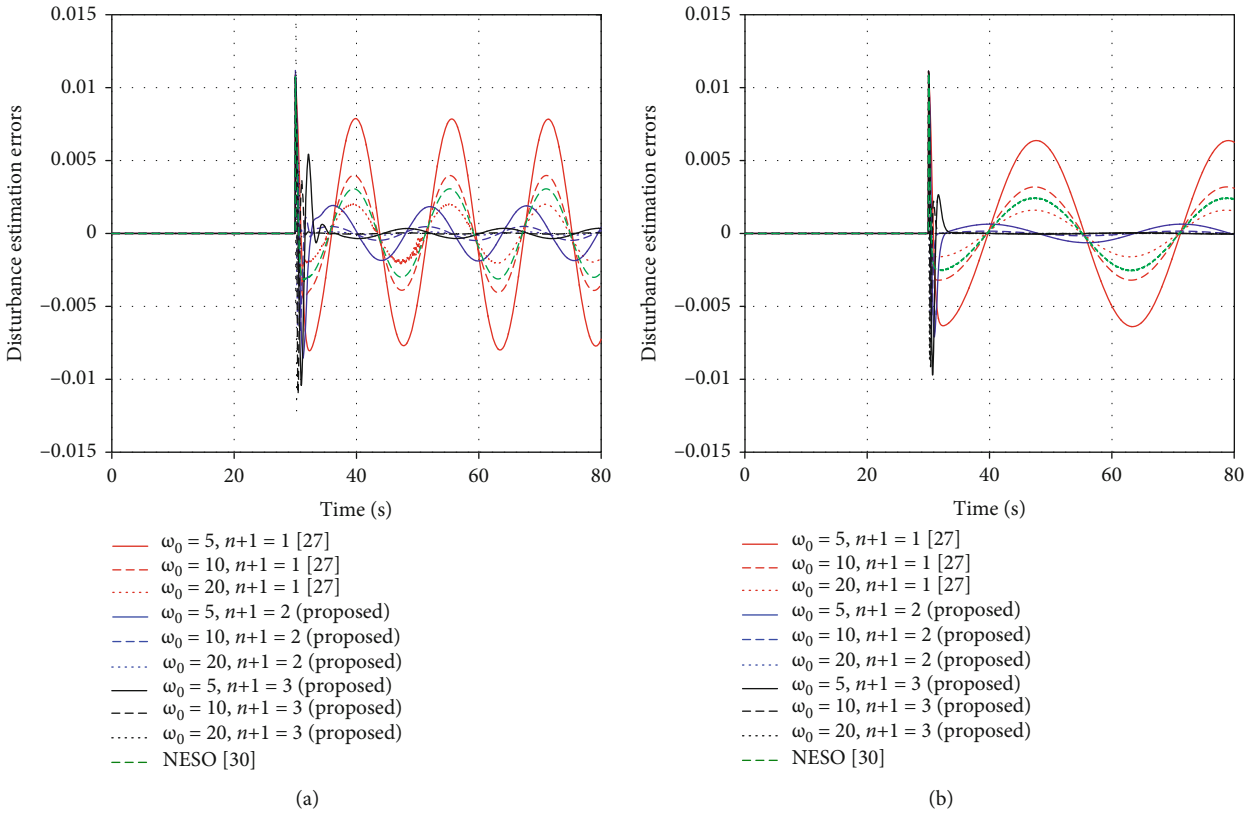

Figure 6: Disturbance estimation errors: (a) velocity channel; (b) altitude channel.

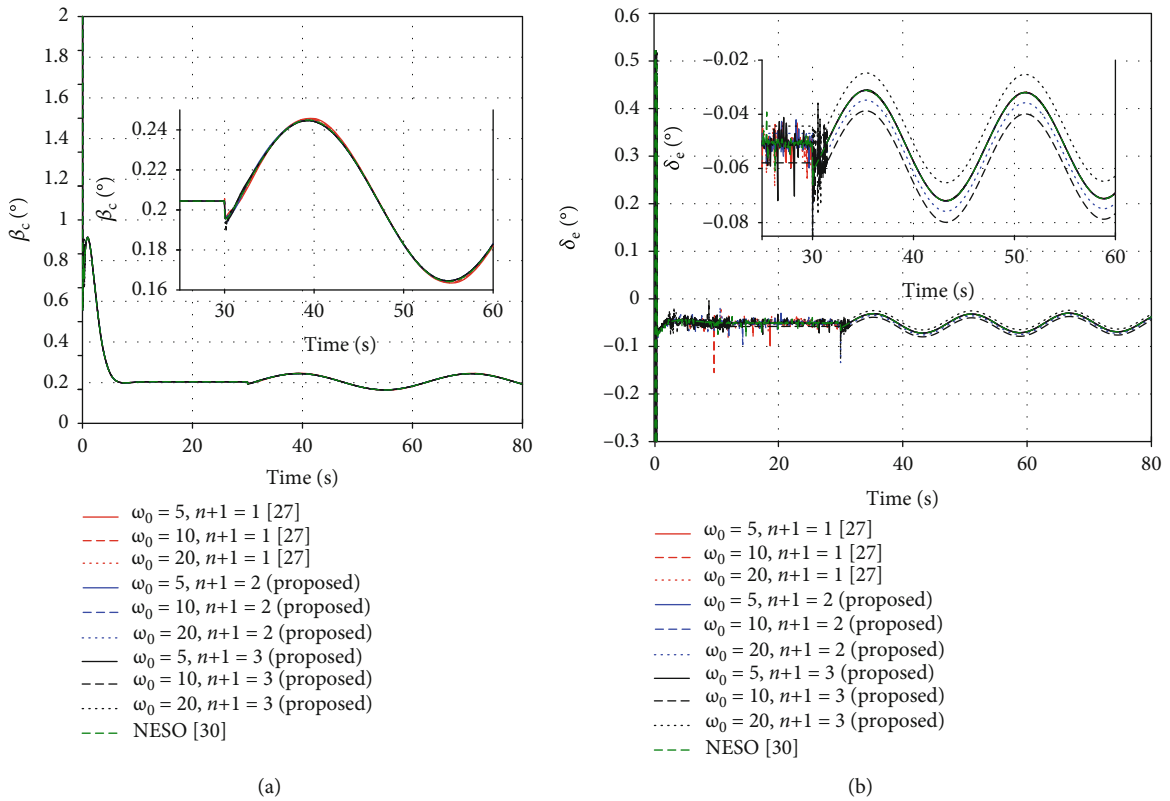

Figure 7: Actuator response curve: (a) throttle setting; (b) elevator deflection.

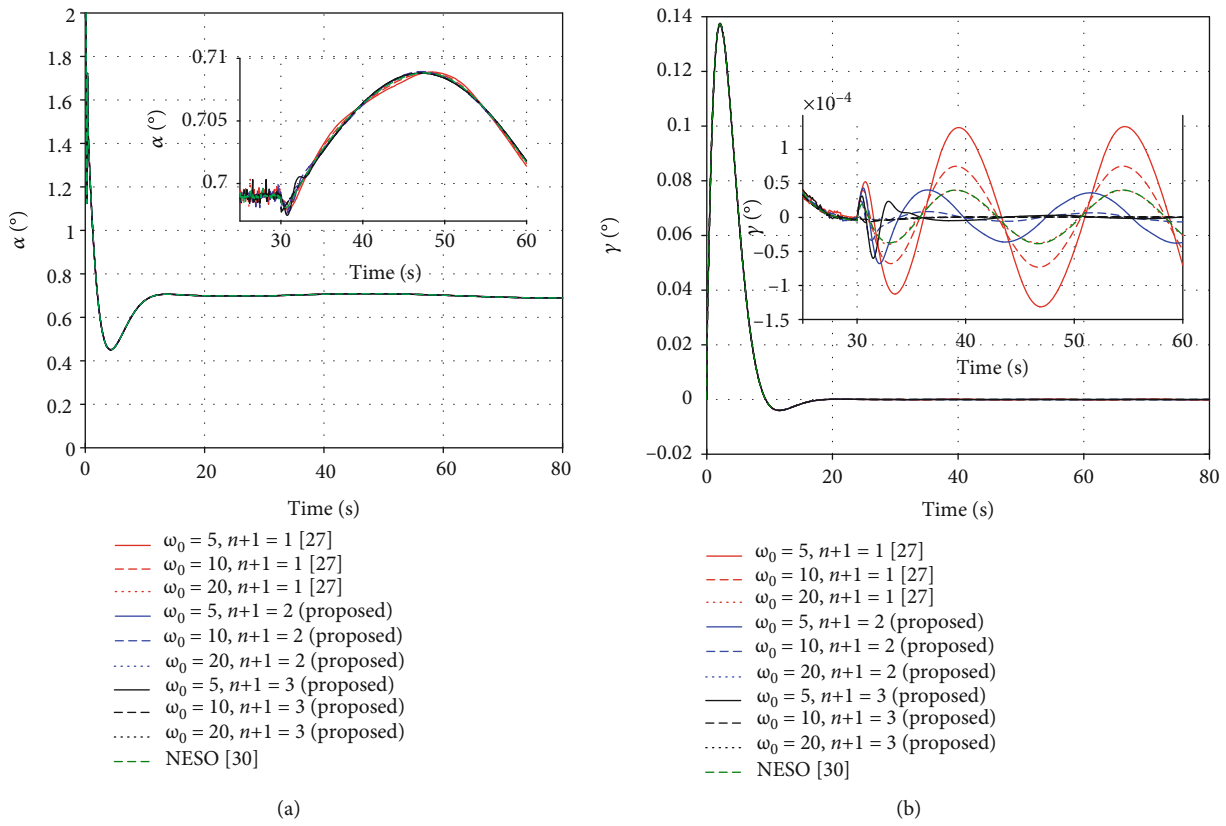

Figure 8: Parametric response curve: (a) attack angle; (b) track angle.

bandwidth, the more serious the situation is. Figure 8 shows the time responses of the attack angle and the track angle. The smaller the observer error is, the smaller the change of attitude angle is, and the better the aircraft stability is. The proposed high-order LESO can improve the system antidisturbance ability by selecting an appropriate order and observer bandwidth. Therefore, for the NSV nonlinear model with uncertain parameters and external disturbance, the simulation results show that the proposed high-order LESO with extended order of 3 and observer bandwidth of 10 is recommendable as the disturbance compensator, which is better than the traditional LESO and the NESO.

5. Conclusions

In this paper, a sliding mode controller with high-order LESO compensation is designed according to the NSV characteristics, which provides a new way to solve uncertain systems with external disturbances. The proposed high-order LESO is suitable for any order system. The transfer function from the lumped disturbance to the disturbance estimates and disturbance estimates error of any order system with any extended order is derived. It can be found that a carefully selected extended order and observer bandwidth can achieve remarkable observer performance gains, more stable system response, and higher steady-state accuracy. However, there are still some other problems need to be solved in the future work, such as the peak phenomenon of intermediate frequency, the high-frequency antidisturbance ability, the different order coupling, and the design of finite-time sliding mode controller. The future work will be focused on how to design the switching control law between the LESO and the NESO, in order to solve the stability problem of multimode switching for near space variable wing vehicle.

Data Availability

The experimental data used to support the findings of this study are available from the corresponding author upon request.

Conflicts of Interest

The authors declare that there are no conflicts of interest regarding the publication of this paper.

Acknowledgments

The authors would like to express their thanks for the support from the Natural Science Foundation of China (No. 61673209, No. 61966010, and No. 81960324).

References

[1] C. Zhang, D. Hu, L. Ye, W. Li, and D. Liu, "Review of the development of hypersonic vehicle technology abroad in 2017," *Tactical Missile Technology*, vol. 39, no. 1, pp. 47–50, 2018.

[2] H. Sun, S. Li, and C. Sun, "Finite time integral sliding mode control of hypersonic vehicles," *Nonlinear Dynamics*, vol. 73, no. 1-2, pp. 229–244, 2013.

[3] R. Zhang, L. Dong, and C. Sun, "Adaptive nonsingular terminal sliding mode control design for near space hypersonic vehicles," *IEEE/CAA Journal of Automatica Sinica*, vol. 1, no. 2, pp. 155–161, 2014.

[4] J. Zhang, J. D. Biggs, D. Ye, and Z. Sun, "Finite-time attitude set-point tracking for thrust-vectoring spacecraft rendezvous," *Aerospace Science and Technology*, vol. 96, article 105588, 2020.

[5] S. Mobayen, M. J. Yazdanpanah, and V. J. Majd, "A finite-time tracker for nonholonomic systems using recursive singularity-free FTSM," in *Proceedings of the 2011 American Control Conference*, pp. 1720–1725, San Francisco, CA, USA, 2011.

[6] J. Sun, J. Yi, Z. Pu, and X. Tan, "Fixed-time sliding mode disturbance observer-based nonsmooth backstepping control for hypersonic vehicles," *IEEE Transactions on Systems, Man, and Cybernetics: Systems*, vol. 50, pp. 4377–4386, 2018.

[7] X. Yin, B. Wang, L. Liu, and Y. Wang, "Disturbance observer-based gain adaptation high-order sliding mode control of hypersonic vehicles," *Aerospace Science and Technology*, vol. 89, pp. 19–30, 2019.

[8] S. Mobayen and F. Tchier, "Nonsingular fast terminal sliding-mode stabilizer for a class of uncertain nonlinear systems based on disturbance observer," *Scientia Iranica*, vol. 24, no. 3, pp. 1410–1418, 2017.

[9] X. Jiao, B. Fidan, J. Jiang, and M. Kamel, "Adaptive mode switching of hypersonic morphing aircraft based on type-2 TSK fuzzy sliding mode control," *Science China Information Sciences*, vol. 58, no. 7, pp. 1–15, 2015.

[10] C. Gu, J. Jiang, and Y. Wu, "Tracking control study of ascent phase for near space vehicle," *Journal of Harbin Engineering University*, vol. 37, no. 11, pp. 1526–1531, 2016.

[11] J. Zhang, D. Ye, J. D. Biggs, Z. Sun, J. D. Biggs, and Z. Sun, "Finite-time relative orbit-attitude tracking control for multi-spacecraft with collision avoidance and changing network topologies," *Advances in Space Research*, vol. 63, no. 3, pp. 1161–1175, 2019.

[12] S. Mobayen, "Design of LMI-based sliding mode controller with an exponential policy for a class of underactuated systems," *Complexity*, vol. 21, no. 5, 2014.

[13] S. Mobayen and J. Ma, "Robust finite-time composite nonlinear feedback control for synchronization of uncertain chaotic systems with nonlinearity and time-delay," *Chaos, Solitons & Fractals*, vol. 114, pp. 46–54, 2018.

[14] J. Zhang, J. D. Biggs, D. Ye, and Z. Sun, "Extended-state-observer-based event-triggered orbit-attitude tracking for low-thrust spacecraft," *IEEE Transactions on Aerospace and Electronic Systems*, vol. 56, pp. 2872–2883, 2020.

[15] M. Cheng, Y. Wu, and F. Ma, "Sliding mode auto-disturbance rejection control of hypersonic vehicle under disturbance," *Journal of System Simulation*, vol. 29, no. 10, pp. 2391–2406, 2017.

[16] H. An, J. Liu, C. Wang, and L. Wu, "Disturbance observer based anti-windup control for air-breathing hypersonic vehicles," *IEEE Transactions on Industrial Electronics*, vol. 63, no. 5, pp. 3038–3049, 2016.

[17] Z. Pu, R. Yuan, J. Yi, and X. Tan, "A class of adaptive extended state observers for nonlinear disturbed systems," *IEEE Transactions on Industrial Electronics*, vol. 62, no. 9, pp. 5858–5869, 2015.

[18] C. Mu, Q. Zong, B. Tian, and W. Xu, "Continues sliding mode controller with disturbance observer for hypersonic vehicles," *IEEE/CAA Journal of Automatica Sinica*, vol. 2, no. 1, pp. 45–55, 2015.

[19] J. Yang, S. Li, C. Sun, and L. Guo, "Nonlinear disturbance observer based robust flight control for airbreathing hypersonic vehicles," *IEEE Transactions on Aerospace and Electronic Systems*, vol. 49, no. 2, pp. 1263–1275, 2013.

[20] A. A. Ball and H. K. Khalil, "High-gain observers in the presence of measurement noise: a nonlinear gain approach," in *2008 47th IEEE Conference on Decision and Control*, pp. 2288–2293, Cancun, Mexico, 2008.

[21] J. P. V. S. Cunha, R. R. Costa, F. Lizarralde, and L. Hsu, "Peaking free variable structure control of uncertain linear systems based on a high-gain observer," *Automatica*, vol. 45, no. 5, pp. 1156–1164, 2009.

[22] X. Shao and H. Wang, "Performance analysis on linear extended state observer and its extention case with higher extended order," *Control and Decision*, vol. 30, no. 5, pp. 815–822, 2015.

[23] B. Fidan, M. Mirmirani, and P. A. Ioannou, "Flight dynamics and control of air-breathing hypersonic vehicles: review and new directions," in *12th AIAA International Space Planes and Hypersonic Systems and Technologies*, Norfolk, Virginia, 2003.

[24] M. A. Bolender and D. B. Doman, "Nonlinear longitudinal dynamical model of an air-breathing hypersonic vehicle," *Journal of Spacecraft and Rockets*, vol. 44, no. 2, pp. 374–387, 2007.

[25] L. Fiorentini, A. Serrani, M. A. Bolender, and D. B. Doman, "Nonlinear robust adaptive control of flexible air-breathing hypersonic vehicles," *Journal of Guidance Control and Dynamics*, vol. 32, no. 2, pp. 402–417, 2009.

[26] J. D. Shaughnessy and S. Z. Pinckney, "Hypersonic vehicle simulation model: winged-cone configuration," in *NASA Technical Memorandum*, USA, 1991NASA TM-102610.

[27] Y. Wu, J. Wang, X. Liu, and Y. Liu, "Disturbance-observer-based sliding mode control for hypersonic flight vehicle," *Control Theory and Applications*, vol. 32, no. 6, pp. 717–724, 2015.

[28] J. Wang, J. Wu, and X. Dong, "Sliding mode control for hypersonic flight vehicle with sliding mode disturbance observer," *Acta Aeronautica et Astronautica Sinica*, vol. 35, pp. 1–8, 2014.

[29] H. Zhang, J. Fan, F. Meng, and J. Huang, "A new sliding control dual power reaching law," *Control and Decision*, vol. 28, no. 2, pp. 289–293, 2013.

[30] J. Chen, D. Nannan, and H. Yu, "Decoupling attitude control of a hypersonic glide vehicle based on a nonlinear extended state observer," *International Journal of Aerospace Engineering*, vol. 2020, Article ID 4905698, 11 pages, 2020.